Aeropropulsive Design Optimization of a Turboelectric Boundary Layer Ingestion Propulsion System

Justin S. Gray *
NASA Glenn Research Center, Cleveland, OH, 44139

Gaetan K.W. Kenway†
Science and Technology Corporation, Moffet Field, CA, 94035

Charles A. Mader‡ and Joaquim R. R. A. Martins §
University of Michigan, Ann Arbor, MI, 48109

Boundary layer ingestion is a coupled aeropropulsive technology that offers the potential for significant improvements to aircraft vehicle performance. NASA's STARC-ABL aircraft configuration is particularly interesting because it leverages boundary layer ingestion with a mostly traditional fuselage. However the design of of STARC-ABL's propulsion systems poses a challenge because the tightly coupled aeropropulsive system is not well handled by traditional uncoupled design methods. To address this we developed a fully coupled aeropropulsive design optimization of the boundary layer ingestion propulsor the STARC-ABL configuration. The integrated model was assembled in the OpenMDAO framework using a three-dimensional RANS CFD aerodynamics model and a one-dimensional thermodynamic propulsion model. The fan for the boundary layer ingestion propulsor was modeled in two parts: a body-force actuator zone is included in the aerodynamics model to produce the thrust and the thermodynamic efficiency of the fan is computed in the propulsion model. The optimization was performed using a gradient based algorithm with the necessary derivatives computed analytically using an adjoint method. The geometry for the aerodynamics model allowed for fine-shape changes of the aft-fuselage, the nacelle walls, and nozzle plug, and for variation of the nacelle diameter. The results show that variations in required thrust also result in different diameters for the optimized propulsor geometries, with fan pressure ratios staying as low as allowed.

Nomenclature

$()_\infty$	free stream quantity
$\hat{\boldsymbol{n}}$	normal vector
ρ	density
$\vec{f}$	local force on an infinitesimal surface element
$\vec{F}$	total force integrated over a surface of volume
A	area
C_F	coefficient of force
C_p	coefficient of pressure
p	static pressure

*Aerospace Engineer PSA Branch, 21000 Brookpark Rd., MS 5-11; Doctoral Candidate Department of Aerospace Engineering, University of Michigan; AIAA Member

†Aerospace Engineer, Science and Technology Corporation; AIAA Senior Member

‡Research Investigator, Department of Aerospace Engineering, AIAA Senior Member

§Professor, Department of Aerospace Engineering; AIAA Associate Fellow

p_t total pressure

V velocity

I. Introduction

Boundary layer ingestion (BLI) for aircraft applications was first proposed by Apollo Smith and Howard Roberts in a 1947 paper that studied the use of jet intakes embedded in the boundary layer as a means to maintain laminar flow and reduce aircraft drag[1]. Aircraft applications for BLI were not examined in further detail initially, but the idea was studied under the term "wake ingestion" for marine applications in the 1960's[2, 3]. In 1993 interest in BLI for aircraft applications was renewed when Leyroy Smith published novel work using a boundary layer analysis, combined with basic propulsion modeling to show the potential for significant fuel burn reduction[4]. Smith identified the tightly coupled aero-propulsive nature of BLI as a key challenge in the analysis and design of the concept. Betz had previously shown that BLI propulsion systems could have a propulsive efficiency of greater than one [5], which made it an ill defined measurement for BLI, so Smith developed a new power based metric to evaluate the performance of BLI propulsion systems called the power saving coefficient (PSC) defined as

$$PSC = \frac{\mathrm{Pwr}'_{\mathrm{shaft}} - \mathrm{Pwr}_{\mathrm{shaft}}}{\mathrm{Pwr}'_{\mathrm{shaft}}}. \tag{1}$$

Significant further work by Drela[6], noting the difficulty of traditional thrust/drag force accounting for BLI systems, proposed an unified power balance accounting scheme that allowed the calculation of the power saving coefficient in a consistent and well defined manner.

A number of conceptual design studies have examined the aircraft level benefits of BLI propulsion systems [7–12], considering a wide range of fuselage and propulsor configuration. The findings of these various papers has demonstrated the potential for BLI to offer significant reductions in aircraft fuel burn; however, the work was all based on uncoupled models of the BLI system. This paper focuses on NASA's STARC-ABL concept, shown in Figure 1, which utilizes a BLI propulsion system with a mostly conventional tube-with-wings layout. The STARC-ABL propulsion system is a turboelectric design consisting of two under-wing turbofan engines with generators attached that transmit power to an electric motor driving the aft-mounted BLI propulsor. Given the layout of the propulsion system, one of the central

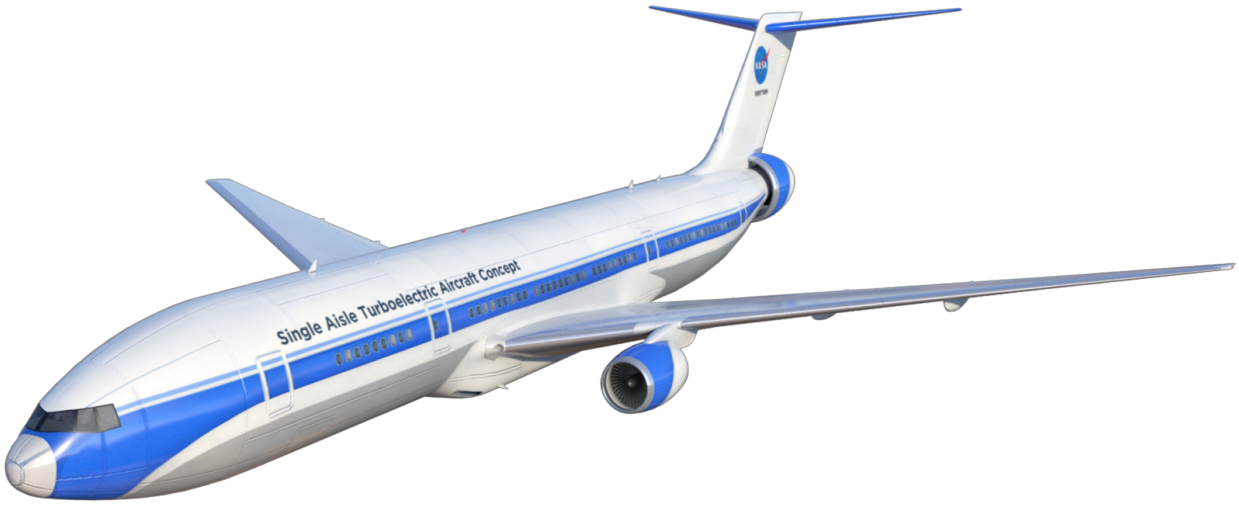

Fig. 1 Rendering of the STARC-ABL aircraft configuration

design questions is the relative size of the two propulsor types to get the best aircraft level performance. Addressing this question requires quantifying the improvement in efficiency of the BLI propulsor vs the under wing engines.

In prior work, we demonstrated the importance of using a fully coupled aeropropulsive model — versus an uncoupled model — to predict BLI performance [13]. We have shown that the coupled model predicts a lower total pressure in the inlet and a different surface pressure distribution on the fuselage compared to an uncoupled model. Furthermore, we

performed a design study focused on the question of relative propulsor sizing, via a series of aeropropulsive design optimizations of the BLI and podded propulsors. Our results showed that the BLI system offered between 1% and 4.5% reduction in total power required for cruise, depending on the assumption made about the power transmission efficiency (η_{trans}) of the turboelectric system. The design study further demonstrated the importance of using a fully coupled aeropropulsive model, and established η_{trans} as a key design assumption for the overall design and performance of the aircraft. However, the aerodynamic models for the previous were constructed from a simplified axisymetric fuselage and BLI propulsor.

While the axisymmetric models were sufficient to establish the fundamental trends, recent aerodynamic analysis of the STARC-ABL configuration has clearly shown that three-dimensional aerodynamic models are necessary in order to accurately predict the airflow at the aft fuselage. Kenway an Kiris examined the inlet distortion for the BLI propulsor on the aft-fuselage of the STARC-ABL configuration [14], concluding that aerodynamic shape optimization reduced distortion to less than 2%. They performed optimizations of both the bare fuselage and a fuselage with wings attached (but without a vertical tail), finding that the wing downwash has a strong impact on the flow and created additional distortion not present in the fuselage only configuration. Beyond the conclusions about distortion, their results clearly demonstrate the importance of using three-dimensional models of the airframe, including the wings, for the aerodynamic analysis. In that work the nacelle design variables only allowed for shape changes at the front section of the nacelle. Significant changes to the nacelle diameter, the shape of the nozzle plug, or to the shape at the aft of the nacelle were not part of the design space. The somewhat limited design freedom present was sufficient for the distortion minimization objective function they used, but was not sufficient to consider large variations in the propulsor sizing.

In this work we perform aeropropulsive design optimization of the BLI propulsor, at a cruise condition of Mach 0.785 and altitude of 37000 ft. The optimization is performed using SNOPT [15], which uses a gradient-based sequential quadratic programming algorithm. The coupled model was constructed in the OpenMDAO framework[16] with a RANS CFD aerodynamic analysis coupled to a 1D thermodynamic cycle model of both the under wing and aft mounted propulsors. All analyses provide analytic derivatives, and OpenMDAO is used to compute the coupled derivatives across the aeropropulsive model.

The propulsor is designed minimize the shaft power required to generate a given net force on the entire aircraft (fuselage, wings, tail, propulsor). At a steady cruise condition the net force on the entire aircraft must be zero, but in this work the aerodynamics model does not include the under-wing engines and hence there will be a non-zero overall net force. Assuming a fixed aircraft geometry, changes in the magnitude of that resulting net force must come from a variation in the thrust produced by the aft BLI propulsor. Distortion is computed using the method developed by Kenway and Kiris, but is not specifically constrained in the optimization. The optimization is run for a series of different propulsor sizes to study the impact of propulsor sizing on BLI performance.

II. Aerodynamic Model

A. RANS Solver: ADflow

The aerodynamic analysis uses the ADflow code, running a RANS analysis [17]. The overset meshes were generated using the Chimera Grid Tools and an implicit hole cutting scheme[18]. The mesh, shown in Figure 2, is composed of 8 different sub-meshes for a total of 6 million cells.

The geometry shown in Figure 2 is modeled with the openVSP geometry engine[19], which outputs a surface discretization for each body in the mesh individually. Then a rigid links interpolation scheme is used to connect the openVSP surface discretization to the surface discretization of the CFD mesh. Changes in the surface mesh are propagated to the volume mesh via an inverse distance weighting implementation of mesh-morphing following the formulation of Luke et al.[18, 20, 21]

The aircraft wing was optimized for minimum drag in prior work, using a 5 point multipoint stencil around the cruise condition [22–24]. The wing geometry was held fixed at this previously optimized design for all studies done in this work. The BLI propulsor is modeled using a body-force zone[25] that imparts the effect of the fan on the flow without needing to model the fan itself. The effect of the body-force zone is highlighted in Figure 3, where contours of total pressure indicate the pressure rise which captures the effect of the fan.

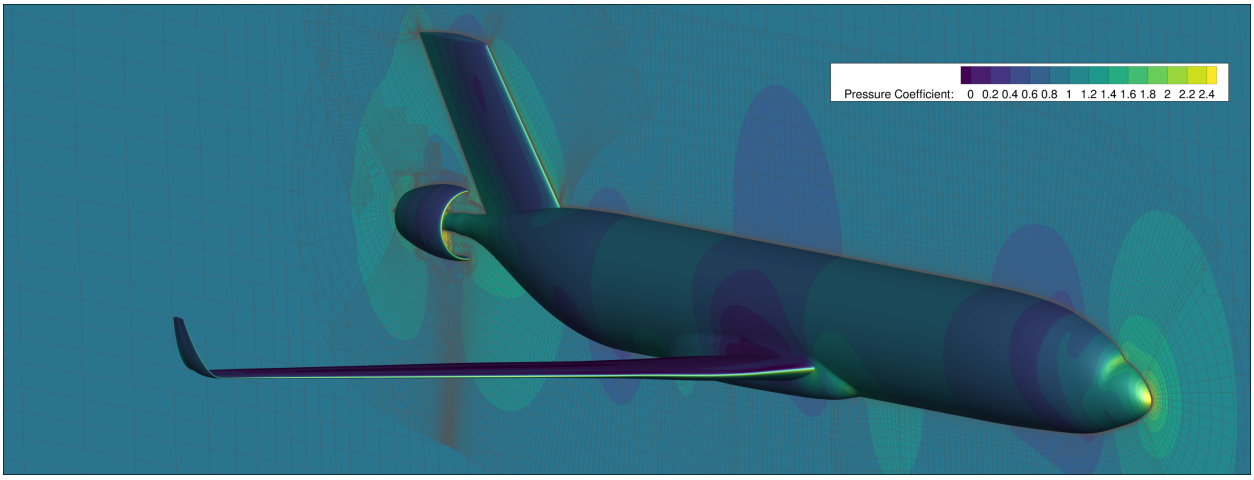

Fig. 2 Overset mesh of of the model with surface C_p color contours.

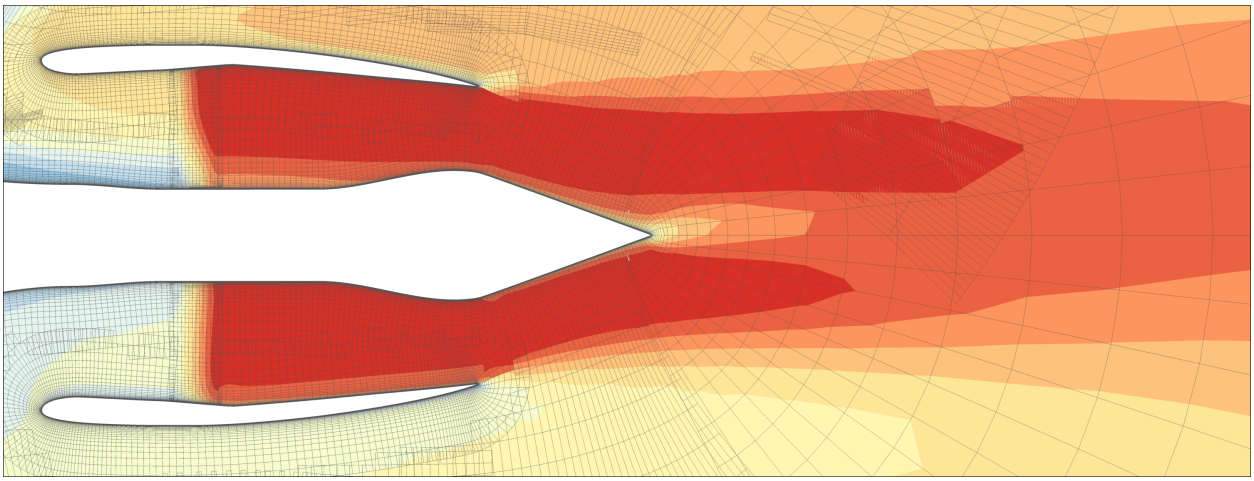

Fig. 3 Side view of the aft mounted BLI propulsor including the body-force zone that simulates the fan. The p_t color contours show the effect of the van via the increased pressure.

Table 1 Reference values for force normalization.

	value	units
ρ_∞	0.3506	kg/m^3
Aref	105.8	m^2
V_∞	231.7	m/s

B. Force Accounting

In typical aircraft analysis the force accounting scheme assumes that the fuselage, wings, and other components create drag and the propulsion system produces thrust. This traditional thrust/drag accounting scheme breaks down for aeropropulsive systems because the interactions between the aerodynamic and propulsion systems makes it impossible to neatly separate out thrust and drag components. This was one of the major motivations for power based accounting schemes like those proposed by Smith [4] and Drela [6].

In this work, when forces are requires, we do not separate out thrusts-drag components at all. Instead, we compute signed force (or force coefficient) values by integrating pressure, viscous, and momentum-flux forces across all the boundaries in the aerodynamics model and adding any force contributions on body-force zones. The total force coefficient on the aircraft is computed by:

$$C_F = \frac{2}{\rho_\infty V_\infty^2 A_{\text{ref}}} \left[\iint_S \left(\left((p - p_\infty)\hat{\boldsymbol{n}} + \vec{\boldsymbol{f}}_{\text{visc}} \right) \right) dS + (\vec{F}_{\text{BLI}} \cdot \hat{\boldsymbol{n}}_{\text{BLI}}) \right]. \tag{2}$$

In equation (2), F_{BLI} represents the force contribution from body-force zone of the aft propulsor. This is not the same as the net thrust from that propulsor, but rather is the net force that would be felt by the fan itself. The integration surface, S, is composed of every surface of the airframe: wing, tail, fuselage, and the inside and outside of the propulsor nacelle. C_F represents the net force coefficient of the entire wing-fuselage-tail-propulsor system, and as such it is a signed quantity. A positive value indicates a net decelerating on the body, while a negative value indicates a net accelerating force on the body. C_F does not include the contribution from the under wing propulsor. For a cruise condition with a constant velocity the net force coefficient of the entire aircraft should be 0, but here C_F is a positive quantity representing a net decelerating force because the under wing propulsor is excluded from the force summation. Effectively, C_F represents the required force coefficient that must be generated by the under wing engines.

At the specified cruise conditions (Mach 0.785 and 37000 ft) the values are used to normalize all force calculations are given in Table 1.

C. Computing BLI Propulsor Power

In order to interface with the propulsion model the power being used by the BLI fan needs to be computed via an volume integral over body-force zone:

$$\text{Pwr}_{\text{flow}} = \iiint \left(\vec{V}_{\text{local}} \cdot \vec{\boldsymbol{f}}_{\text{local}} \right) dv, \tag{3}$$

where V_{local} is the local velocity vector and $\vec{\boldsymbol{f}}_{\text{local}}$ is the local body-force contribution for the infinitesimal fluid volume.

Note that Equation (3) computes only the power imparted to the flow by the fan, which does not equal the total shaft power needed to drive the fan. The shaft power and the flow power differ because of the fan adiabatic efficiency, η_{fan}. Thermodynamically, η_{fan} causes a slight increase in temperature of the flow, relative to what you would expect for ideal case. The implementation of the body-force zone used in this work assumes an isentropic pressure rise, based on the formulation of Hall et. al. [25]. Since the pressure ratio of the fan is so small, the lack of the temperature rise in the flow does not introduce major aerodynamic error. However the effect is significant to the propulsion system, which must ultimately provide the necessary shaft power, so η_{fan} is accounted for in the propulsion model.

III. Propulsion Model

A. 1D Cycle Model: pyCycle

The propulsion model used is a one-dimensional thermodynamic cycle model, built with pyCycle[26, 27]. pyCycle is a modular cycle modeling tool similar to the industry standard NPSS[28] with the added feature of analytic derivative computation for use in optimization applications. Propulsion models are built up from cycle elements such as *Compressor Turbine*, *Combustor*, *Nozzle*, etc.

The one-dimensional propulsion model requires scalar flow quantities as inputs, but the aerodynamic analysis computes the flow quantities as a nonuniform distribution over a two-dimensional plane. At the interface between the aerodynamic analysis and the propulsion model the two-dimensional data needs to be averaged into equivalent one-dimensional values, but it is important for this process to be done in a conservative fashion so that the correct net force on the boundary is retained in both analyses.

There are a number of different approaches to do this averaging, which conserve different flow quantities. Livesey [29, 30] compared a number of different methods, from the perspective of computing scalar values from rake data measured in a experiment, concluding that an entropy conserving approach was the most useful in that context because that ensured that physically meaningful pressure loss coefficients are computed when the averaged values are compared at multiple axial locations.

In this application, the interface plane represents a transition from one analysis to another and the principal concern is that the net force on the interface plane is the same between the two analyses. The forces are governed by the static pressure and momentum flux through the interface plane, so these are the quantities we seek to conserve.

In the aerodynamic analysis, the force normal to any plane is computed by

$$F_S = \iint_S \left[(p - p_\infty) + \rho(V - V_\infty)(\vec{V} \cdot \hat{\boldsymbol{n}}) \right] dS. \tag{4}$$

If we assume uniform values across the plane, so the flow can be represented by scalar values, Equation (4) simplifies to

$$F_S = \left[(\bar{p} - p_\infty) A_S + \dot{m} \left(\bar{V} - V_\infty \right) \right] \hat{\boldsymbol{n}}. \tag{5}$$

Over any given plane, the total mass flow rate and area can be computed via

$$\dot{m} = \iint_S \rho \vec{V} \cdot \hat{n} dS, \tag{6}$$

$$A = \iint_S dS. \tag{7}$$

Equating Equations (4) and (5), canceling out the p_∞ and V_∞ terms, and separating the pressure and velocity components yields

$$\bar{p} = \frac{1}{A} \iint_S p dS, \tag{8}$$

$$\bar{V} = \frac{1}{\dot{m}} \iint_S V \rho (\vec{V} \cdot \hat{\boldsymbol{n}}) dS \tag{9}$$

These equations show that a force-conserving averaging scheme requires the inflow conditions to the propulsion model should be chosen such that the static pressure matches the area averaged static pressure, and the flow velocity should match the mass averaged velocity on the interface plane.

B. BLI Propulsor Model

Although the thrust from the BLI propulsor is modeled as via a body-force actuator zone in the aerodynamics model, a propulsion model is still needed to compute the shaft power required to produce that thrust. The BLI propulsor model is composed of four cycle elements: *CFD Start*, *Ambient*, *Fan*, and *Performance*.

The *CFD Start* element uses a nonlinear solver to implement the force conserving flow averaging scheme described previously. The implicit variables p_t, T_t, MN are solver for such that the static conditions match the computed $\bar{P}_s, \bar{V}, A$ for a given $\dot{m}$. The *Ambient* component uses a 1976 standard atmosphere to compute the freestream flow properties.

The *Fan* and *Performance* handle the actual thermodynamic calculations that compute a required shaft power from the $\dot{m}$ and pressure ratio computed by the aerodynamic analysis. Figure 4 shows the connections between the four cycle elements of this model.

The fan efficiency is computed such that the polytropic efficiency, η_{poly}, is held constant at 97%, which matches the technology assumptions for NASA's N+3 high bypass ratio turbofan engine [31]. The effect of holding a constant η_{poly} is that the adiabatic efficiency of the fan, $\eta_{\text{adiabatic}}$, — the quantity that directly impacts the shaft power— varies with respect to fan pressure ratio (FPR) and is always less than 97%. The resulting variation of $\eta_{\text{adiabatic}}$ is nearly linear because of the very low FPR, as shown in Fig. 5. The trend.

This model outputs the required generator power, which takes into account both the fan efficiency ($\eta_{\text{adiabatic}}$) and the power transmission efficiency (η_{trans}). The required generator power becomes an input to the under-wing engines, which includes it as an additional load on the lower pressure spool.

IV. Aeropropulsive Optimization

A. Optimization Problem

The performance of the BLI system was analyzed at the cruise condition, Mach 0.785 and 37000 ft. For a steady cruise, there will be zero net force over the entire aircraft, including the under-wing propulsors, wings, tail, fuselage, and aft-propulsor. A portion of the thrust will come from the under-wing propulsor and a portion from the aft-propulsor. One primary consideration in the propulsion system design is what the optimal split between the under-wing and aft propulsors should be to achieve the lowest overall fuel consumption. For a full aircraft design process addressing this question requires other considerations, such as thermodynamic performance, propulsion system weight, and aircraft center of gravity. In this work we have modeled only the thermodynamic performance of the aft-propulsor, and hence we cannot fully address this design question. However, in recognition of the importance of propulsor sizing to the overall aircraft performance we consider optimized designs of BLI propulsors for three different sizes and compare their relative performance.

Each optimization was formulated to minimize the shaft power required by the BLI propulsor at the cruise condition with respect to fusleage shape design variables and propulsion design variables, subject to set of constraints. The full problem formulation is given in Table 2, which describes the 26 design variables and 14 constraints. Of the 14 constraints, the F_{net} constraint is the most physically significant because that is what ultimately sizes the BLI propupulsor. The 10 geometric thickness constraints are cheap to evaluate because they do not involve the CFD analysis at all, so overall, the problem requires just four expensive adjoints. The use of the nozzle pressure ratio constraint is notable here, because it is not normally used to govern the design of a fan. In this work, the NPR constraint was used in lieu of a constraint on FPR because it was more well behaved for shape optimization of the propulsor duct.

Using a sign convention derived from the aerodynamic model with the origin located at the aircraft nose, positive values of net force represent a decelerative force on the body. Since the aerodynamic model only includes the aft propulsor, the F_{net} value computed from it represents the amount of net thrust required from the under-wing propulsors for a steady cruise condition. A larger F_{net} indicates larger under-wing propulsors and a smaller aft-propulsor.

Figure 6 shows the XDSM[32] of the optimization formulation, indicating how data is passed between the different analyses. The four different analyses are coupled using OpenMDAO, which both solves the nonlinear analysis and computes the total derivatives needed by the optimizer using an adjoint formulation.

In Figure 6, there is a component labeled *VSP Preprocessing*. The geometry engine for this work is OpenVSP, which is integrated directly inside the *ADflow* discipline. OpenVSP exposes a number of parameters that control the shape and

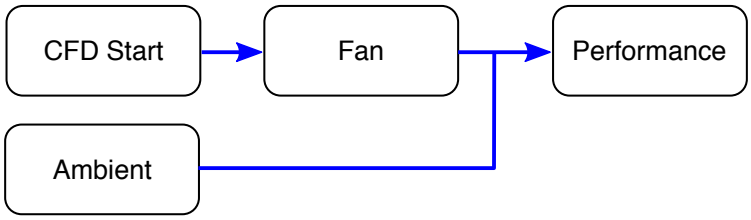

Fig. 4 Cycle elements in the pyCycle model of the BLI propulsor.

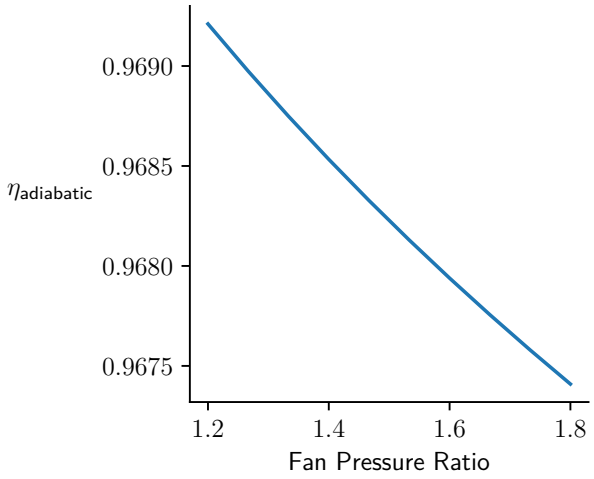

Fig. 5 Fan adiabatic efficiency versus FPR, assuming a constant polytropic efficiency of 97%.

Table 2 Optimization problem definition for the aero-propulsive design of the propulsion system.

	Variable/Function	Description	Quantity
minimize	$\text{Pwr}_{\text{BLI-shaft}}$	Shaft power required for the BLI propulsor	
with respect to	F_{BLI}	BLI propulsor body-force applied	1
	X_{shape}	Fuselage and propulsor nacelle shape variables	25
		Total	26
subject to	$C_L = 0.5$	Lift coefficient at cruise	1
	$0.99 < g_{\text{geo}} < 3.0$	Geometric thickness constraints	10
	NPR > 1.65	Nozzle pressure ratio constraint	1
	$F_{\text{net}} = F^*_{\text{net}}$	Required net force on the body	1
		Total	14

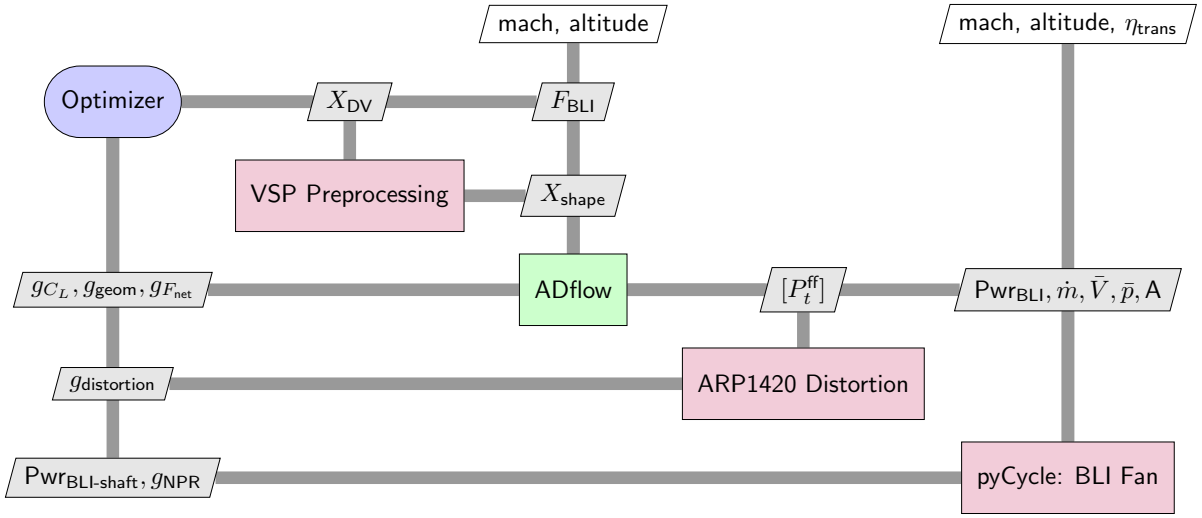

Fig. 6 XDSM diagram of the full optimization problem formulation.

diameters of cross-sections on both the fuselage, BLI nacelle, and wing. However, for this work, a number of those parameters were linked together to provide a more physically meaningful geometry parameterization. For example, in the OpenVSP model the sharp trailing edge of the nacelle is parameterized with two separate diameters: one for the upper surface and one for the lower surface. It is important that both these diameters are always forced to take the same value, so the geometry stays water tight. This is accomplished via the *VSP Preprocessing* component in the model, which takes a set of design variables and relates them to the actual OpenVSP model inputs.

The *ARP1420 Distortion* component implements the distortion metric from the "Gas Turbine Engine Inlet Flow Distortion Guidelines" ARP1420 standard[33], using the scheme developed by by Kenway and Keris [14]. The metric captures the magnitude of the variation in total pressure across the fan face both circumferentially and radially using data taken from multiple sensor locations distributed across the fan face. We use five radial measurement locations each with 30 sensors distributed evenly in the circumferential direction, yielding a total of 150 sensors. The five distortion measurements from each of the five radii are aggregated with a KS function [34], giving a smoothed maximum value thats can be used as a constraint on the optimization. In this work, the distortion was computed but not directly constrained.

B. Optimization Results

Three optimizations were performed for F_{net}^* values of 9000 N, 11000 N, and 13000 N. Key performance parameters from each optimization are reported in Table 3. The 9000 N case yields the largest aft-propulsor and hence requires the most shaft power. Compared to the 9000 N case, the 11000 N case requires 22% more thrust from the under-wing propulsors and uses 14.6% less shaft power for the BLI propulsor. The 13000 N case requires 44% more thrust from the under-wing propulsors and uses 29.2% less shaft power for the aft propulsor. For all three cases, the constraint on NPR limits the fan pressure ratio from going below about 1.3.

The total pressure recovery, $p_t/p_{t\infty}$, and the distortion metric give somewhat inconclusive trends. The maximum pressure recovery and the minimum distortion both occur for the 11000 Newton case. The inlet total pressure recovery is notable here though, with an average value of 86.1% between all three cases. For a typical free stream podded propulsor, a pressure recovery of closer to 98% would be expected. If such relatively lower total pressure air was to be ingested by turbomachinery, it would have an extremely deleterious effect on the overall thermal efficiency of the cycyle. STARC-ABL is still affected by the total pressure loss via a relatively lower NPR for the same FPR, but since there is no engine core the negative impact on overall thermodynamic efficiency does not manifest.

Figure 7 shows the side and front views of the baseline and optimized geometries for the three F_{net}^* cases. The color contours show the total pressure levels around the aircraft, where the front view contours highlight the distortion in the inlet for the BLI propulsors. In all three optimized cases, we can see a more severe nozzle contraction being used to improve the overall thrust. In addition, some shaping on the nozzle plug also helps alleviate some minor flow separation

Table 3 Performance data for optimized BLI propulsor designs for a range of different F_{net} values.

$C_F \times 10^4$	FPR	$p_t/p_{t\infty}$	BLI shaft power (kW)	Distortion metric
90.39	1.30	0.845	2437	0.030
110.5	1.32	0.872	2081	0.027
130.6	1.32	0.867	1725	0.037

and yield slightly better overall performance. Compared to the baseline geometry, the nacelle walls are thicker near the leading edge and much thinner near the trailing edge compared to the baseline. The pressure contours also indicate that the flow is more uniform exiting the nozzle in the optimized cases.

All cases (baseline and three optimized geometries) have a zone of higher total pressure at the bottom of the BLI propulsor inlet. This would create a one-per-revolution excitation in the fan blades and that would require careful aerostructural design. In future work, distortion will be implemented as optimization constraint, and the geometric freedom of the model will be used to try to alleviate the distortion and make the flow more uniform circumferentially.

V. Conclusions

This paper presents the aeropropulsive design optimization of a BLI propulsor for NASA's STARC-ABL aircraft, using a RANS CFD aerodynamics model coupled to a one-dimensional thermodynamic cycle model for the BLI fan. The coupled model was constructed using the OpenMDAO framework, which enabled the computation of analytic derivatives for efficient gradient based optimization.

The optimization sought to minimize the BLI propulsor shaft power required at a cruise condition of Mach 0.785 and 37000 ft. The aerodynamic model included the fuselage, tail, BLI propulsor, and wing. A distortion metric based on the ARP-1420 inlet standard was included as a computed quantity, but not directly constrained as part of the optimization. The propulsion model included a variation in fan efficiency as a function of fan pressure ratio. The aeropropulsive coupling was accomplished via a new flow-averaging scheme that conserves force and energy flow across the interface plane between the aerodynamics and propulsion.

Three optimizations were run for different values of the constraint on the net force over the whole body, F_{net}, representing three different sized propulsors. The optimized results all found the lowest FPR allowed by the constraints on the problem, choosing to vary the nacelle diameter to accomplish the change in required force from the propulsor. All results showed a noticeable distortion pattern due to the three-dimensional aerodynamics, including effects from the vertical tail and the wing downwash. Future work will add a constraints on distortion to the optimization problem to leverage the shape optimization to mitigate some of the distortion effects.

This work represents a step toward aeropropulsive design optimization of a full aircraft propulsion system. The next step is to integrate a full under wing propulsor model and run optimizations of the full aircraft configuration.

VI. Acknowledgments

The authors would like to thank the NASA Transformational Tools and Technologies Project and the Advanced Air Transport Technologies Project for supporting this work. We would also like to thank Dr. Eric Hendricks the many thoughtful discussions about boundary layer ingestion and propulsion airframe integration.

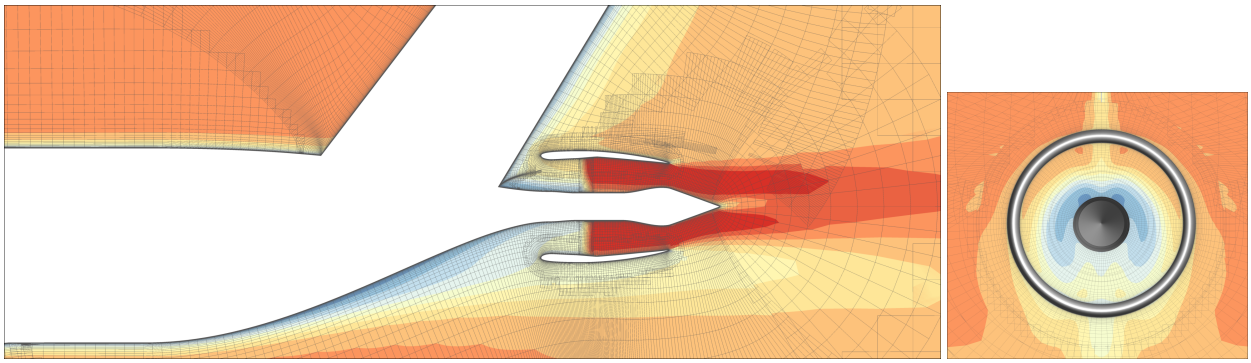

(a) Baseline Geometry

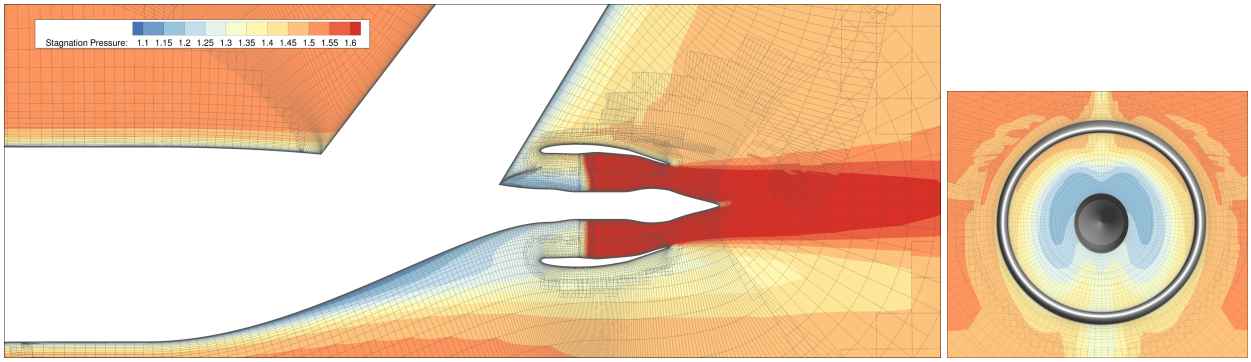

(b) C_F = .009039

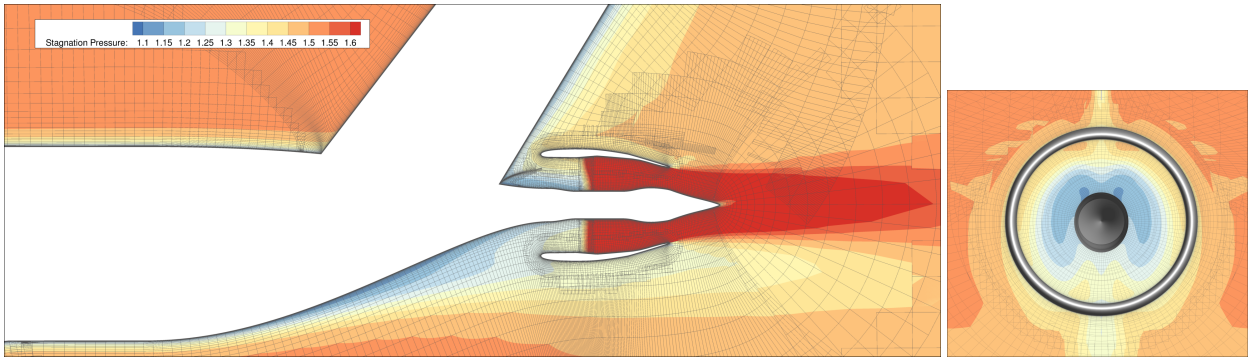

(c) C_F = 0.01105

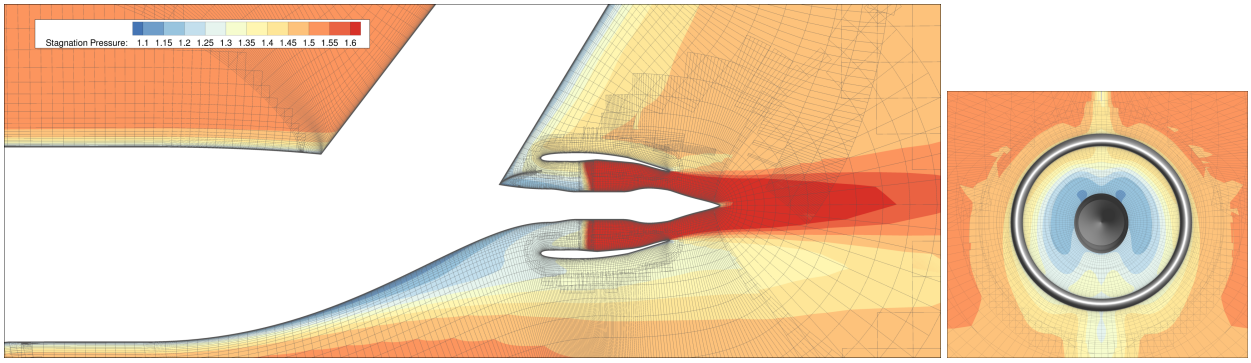

(d) C_F = 0.01306

Fig. 7 Contours of stagnation pressure for the baseline and three optimized geometries.

References

[1] Smith, A. M. O., and Roberts, H. E., "The Jet Airplane Utilizing Boundary Layer Ingestion for Propulsion," *Journal of Aeronautical Sciences*, Vol. 14, No. 2, 1947, pp. 97–109.

[2] Wislicenus, G. F., "Hydrodynamics and Propulsion of Submerged Bodies," *Journal of the American Rocket Society*, Vol. 30, 1960, pp. 1140–1148.

[3] Gearhart, W. S., and Henderson, R. E., "Selection of a Propulsor for a Submersible System," *Journal of Aircraft*, Vol. 3, No. 1, 1966, pp. 84–90.

[4] Smith, L. H., "Wake Ingestion Propulsion Benefit," *Journal of Propulsion and Power*, Vol. 9, No. 1, 1993, pp. 74–82. doi:10.2514/6.1991-2007.

[5] Betz, A., *Introduction to the Theory of Flow Machines*, Pergamon Press, 1966.

[6] Drela, M., "Power Balance in Aerodynamic Flows," *AIAA Journal*, Vol. 47, No. 7, 2009, pp. 1761–1771. doi:10.2514/1.42409.

[7] Daggett, D. L., Kawai, R., and Friedman, D., *Blended Wing Body Systems Studies: Boundary Layer Ingestion Inlets With Active Flow Control*, 2003. NASA CR-2003-212670.

[8] Felder, J. L., Kim, H. D., and Brown, G. V., "Turboelectric Distributed Propulsion Engine Cycle Analysis for Hybrid-Wing-Body Aircraft," *47th AIAA Aerospace Sciences Meeting including The New Horizons Forum and Aerospace Exposition*, 2009. doi:10.2514/6.2009-1132, aIAA 2009-1132.

[9] Drela, M., "Development of the D8 Transport Configuration," *9th AIAA Applied Aerodynamics Conference*, 2011. doi:10.2514/6.2011-3970, aIAA 2011-3970.

[10] Liu, C., Doulgeris, G., Laskaridis, P., and Singh, R., "Thermal cycle analysis of turboelectric distributed propulsion system with boundary layer ingestion," *Aerospace Science and Technology*, Vol. 27, No. 1, 2013, pp. 163 – 170. doi:http://dx.doi.org/10.1016/j.ast.2012.08.003.

[11] Laskaridis, P., Pachidis, V., and Pilidis, P., "Opportunities and challenges for distributed propulsion and boundary layer ingestion," *Aircraft Engineering and Aerospace Technology*, Vol. 86, No. 6, 2014, pp. 451–458. doi:10.1108/AEAT-05-2014-0067.

[12] Welstead, J. R., and Felder, J. L., "Conceptual Design of a Single-Aisle Turboelectric Commercial Transport with Fuselage Boundary Layer Ingestion," *54th AIAA Aerospace Sciences Meeting*, 2016. doi:10.2514/6.2016-1027, aIAA 2016-1027.

[13] Gray, J. S., Mader, C. A., Kenway, G. K. W., and Martins, J. R. R. A., "Modeling Boundary Layer Ingestion Using a Coupled Aeropropulsive Analysis," *AIAA Journal of Aircraft*, 2017. doi:10.2514/1.C034601.

[14] "Aerodynamic shape optimization of the STARC-ABL concept for minimal inlet distortion," , January 2018. doi:10.2514/6.2018-1912.

[15] Gill, P. E., Murray, W., and Saunders, M. A., "SNOPT: An SQP Algorithm for Large-Scale Constrained Optimization," *SIAM Rev.*, Vol. 47, No. 1, 2005, pp. 99–131. doi:10.1137/S0036144504446096, URL `http://dx.doi.org/10.1137/S0036144504446096`.

[16] Gray, J. S., Hearn, T. A., Moore, K. T., Hwang, J. T., Martins, J. R. R. A., and Ning, A., "Automatic Evaluation of Multidisciplinary Derivatives Using a Graph-Based Problem Formulation in OpenMDAO," *15th AIAA/ISSMO Multidisciplinary Analysis and Optimization Conference*, American Institute of Aeronautics and Astronautics, 2014. doi:10.2514/6.2014-2042.

[17] Kenway, G. K. W., Secco, N. R., Martins, J. R. R. A., Mishra, A., and Duraisamy, K., "An Efficient Parallel Overset Method for Aerodynamic Shape Optimization," *Proceedings of the 58th AIAA/ASCE/AHS/ASC Structures, Structural Dynamics, and Materials Conference, AIAA SciTech Formum*, 2017. doi:10.2514/6.2017-0357.

[18] Secco, N. R., Jasa, J. P., Kenway, G. K. W., and Martins, J. R. R. A., "Component-based Geometry Manipulation for Aerodynamic Shape Optimization with Overset Meshes," *18th AIAA/ISSMO Multidisciplinary Analysis and Optimization Conference*, 2017.

[19] Hahn, A., "Vehicle Sketch Pad: a Parametric Geometry Modeler for Conceptual Aircraft Design," *48th AIAA Aerospace Sciences Meeting Including the New Horizons Forum and Aerospace Exposition, Aerospace Sciences Meetings*, 2010. AIAA 2010-657.

[20] Luke, E., Collins, E., and Blades, E., "A fast mesh deformation method using explicit interpolation," *Journal of Computational Physics*, Vol. 231, No. 2, 2012, pp. 586 – 601. doi:10.1016/j.jcp.2011.09.021.

[21] Brooks, T. R., Kenway, G. K. W., and Martins, J. R. R. A., "uCRM: An Aerostructural Model for the Study of Flexible Transonic Aircraft Wings," *AIAA Journal*, 2018. (In press).

[22] Kenway, G. K. W., and Martins, J. R. R. A., "Multipoint Aerodynamic Shape Optimization Investigations of the Common Research Model Wing," *AIAA Journal*, Vol. 54, No. 1, 2016, pp. 113–128. doi:10.2514/1.J054154.

[23] Liem, R. P., Kenway, G. K., and Martins, J. R. R. A., "Multi-point, multi-mission, high-fidelity aerostructural optimization of a long-range aircraft configuration," *Proceedings of the 14th AIAA/ISSMO Multidisciplinary Analysis and Optimization Conference*, Indianapolis, IN, 2012. doi:10.2514/6.2012-5706.

[24] Liem, R. P., Kenway, G. K. W., and Martins, J. R. R. A., "Multimission Aircraft Fuel Burn Minimization via Multipoint Aerostructural Optimization," *AIAA Journal*, Vol. 53, No. 1, 2015, pp. 104–122. doi:10.2514/1.J052940.

[25] Hall, D. K., Greitzer, E. M., and Tan, C. S., "Analysis of Fan Stage Design Attributes for Boundary Layer Ingestion," *ASME. Turbo Expo: Power for Land, Sea, and Aif; Volume 2A: Turbomachinery*, 2016. doi:10.1115/GT2016-57808.

[26] Gray, J., Chin, J., Hearn, T., Hendricks, E., Lavelle, T., and Martins, J. R. R. A., "Chemical Equilibrium Analysis with Adjoint Derivatives for Propulsion Cycle Analysis," *Journal of Propulsion and Power*, Vol. 33, No. 5, 2017, pp. 1041–1052. doi:10.2514/1.B36215.

[27] Hearn, D. T., Hendricks, E., Chin, J., Gray, J., and Moore, D. K. T., "Optimization of Turbine Engine Cycle Analysis with Analytic Derivatives," *17th AIAA/ISSMO Multidisciplinary Analysis and Optimization Conference, part of AIAA Aviation 2016 (Washington, DC)*, 2016. doi:10.2514/6.2016-4297.

[28] Jones, S., *An Introduction to Thermodynamic Performance Analysis of Aircraft Gas Turbine Engine Cycles Using the Numerical Propulsion System Simulation Code*, 2007. NASA TM-2007-214690.

[29] Livesey, J. L., and Hugh, T., "'Suitable Mean Values' in One-Dimensional Gas Dynamics," *Journal of Mechanical Engineering Science*, Vol. 8, No. 4, 1966, pp. 374–383. doi:10.1243/JMES_JOUR_1966_008_049_02.

[30] Livesey, J. L. (ed.), *Flow property averaging methods for compressible internal flows*, 1982. doi:10.2514/6.1982-135.

[31] Jones, S. M., Haller, W. J., and Tong, M. T., *An N+3 Technology Level Reference Propulsion System*, 2017. NASA/TM—2017-219501.

[32] Lambe, A. B., and Martins, J. R. R. A., "Extensions to the Design Structure Matrix for the Description of Multidisciplinary Design, Analysis, and Optimization Processes," *Structural and Multidisciplinary Optimization*, Vol. 46, 2012, pp. 273–284. doi:10.1007/s00158-012-0763-y.

[33] International, S., *Gas turbine inlet flow distortion guidelines. Aerospace Recommended Practice ARP1420*, 2017.

[34] Kreisselmeier, G., and Steinhauser, R., "Systematic Control Design by Optimizing a Vector Performance Index," *International Federation of Active Controls Symposium on Computer-Aided Design of Control Systems, Zurich, Switzerland*, 1979.